Signature of Cascade Transitions between Interlayer Excitons in a Moiré Superlattice

Qinghai Tan,[1,2,*] Abdullah Rasmita,[1,*] Zhaowei Zhang,[1] K. S. Novoselov,[3,†] and Wei-bo Gao[1,2,4,‡]

[1]*Division of Physics and Applied Physics, School of Physical and Mathematical Sciences, Nanyang Technological University, Singapore 637371, Singapore*

[2]*The Photonics Institute and Centre for Disruptive Photonic Technologies, Nanyang Technological University, Singapore 637371, Singapore*

[3]*Department of Materials Science and Engineering, National University of Singapore, 9 Engineering Drive 1, 117575, Singapore*

[4]*Centre for Quantum Technologies, National University of Singapore, 117543 Singapore, Singapore*

(Received 18 June 2022; accepted 8 November 2022; published 5 December 2022)

A moiré superlattice in transition metal dichalcogenides heterostructure provides an exciting platform for studying strongly correlated electronics and excitonic physics, such as multiple interlayer exciton (IX) energy bands. However, the correlations between these IXs remain elusive. Here, we demonstrate the cascade transitions between IXs in a moiré superlattice by performing energy- and time-resolved photoluminescence measurements in the MoS_2/WSe_2 heterostructure. Furthermore, we show that the lower-energy IX can be excited to higher-energy ones, facilitating IX population inversion. Our finding of cascade transitions between IXs contributes to the fundamental understanding of the IX dynamics in moiré superlattices and may have important applications, such as in exciton condensate, quantum information protocols, and quantum cascade lasers.

DOI: 10.1103/PhysRevLett.129.247401

Moiré superlattice can emerge when two different two-dimensional (2D) van der Waals crystals are stacked on top of each other [1–5]. Similar to the superlattice in the multiple quantum well (MQW) system [6], the moiré superlattice can result in the creation of electron minibands [7–14]. Compared to MQW, the fabrication of 2D heterostructure is simpler since it does not involve epitaxial methods necessary for the former one [15]. Moreover, the interlayer twist angle can modulate the moiré superlattice potential [7], which adds another degree of freedom to the superlattice design.

For optoelectronics applications, the transition metal dichalcogenides (TMDs) are one of the most promising 2D materials due to their direct band gap at the monolayer limit and the strong light-matter interactions [16,17]. The optical emission in these materials is dominated by the exciton (i.e., bound electron-hole pair) [18]. Similar to the electron case, the moiré superlattice in the TMD heterobilayer has been shown to create the minibands for both intralayer (electron and hole in the same layer) [19–22] and interlayer (electron and hole in different layers) exciton [20,22–25]. Such minibands result in multiple emission and absorption peaks [19–28]. Regarding the interlayer exciton (IX), its long lifetime and large binding energy are advantageous for realizing high-temperature Bose-Einstein condensate [29]. Moreover, the confinement provided by the moiré potential can result in the IX quantum emitter array [26,30].

The existence of multiple IX minibands in the 2D TMD moiré superlattice raises the question of whether there are transitions between these minibands, resulting in a cascade transition (i.e., one transition followed by another one) to the ground state. Detection of cascade transition may indicate that the multiple IXs originate from one location [23,24] instead of multiple locations [26] in the moiré superlattice. When it is radiative, cascade transition may result in entangled photon emission [31,32] and is an important ingredient for quantum cascade lasers (QCL) [33,34].

In this Letter, we utilized energy- and time-resolved photoluminescence (PL) measurements to study the transition between IXs in a MoS_2/WSe_2 moiré superlattice. We observed multiple peaks in the IX PL from the monolayer-MoS_2/monolayer-WSe_2 sample and studied the time-resolved PL of individual peaks. By analyzing the time-resolved data, we demonstrated the cascade transition between the IX energy levels. Additionally, we show that it is possible to excite the lower-level IXs to a high-energy state which decays quickly to the higher-level IXs, effectively creating a three-level system—the minimum requirement for population inversion.

Figure 1(a) shows the optical microscope of one MoS_2/WSe_2 sample consisting of monolayer MoS_2 and WSe_2 encapsulated by hexagonal boron nitride (*h*-BN). Based on the second harmonic generation measurement, we determine that the heterobilayer are *AB* stacked [i.e., with a twist angle of ~60°, see Fig. S1(a) in Supplemental Material (SM) [35]]. Since there is a significant lattice mismatch between the layers, the moiré superlattice in MoS_2/WSe_2 heterostructure is less sensitive to the twist

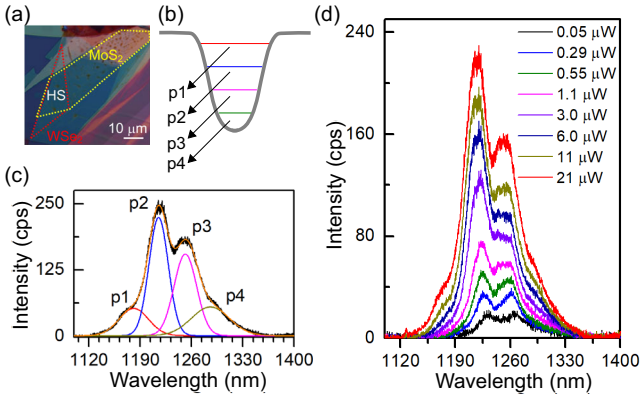

FIG. 1. (a) Optical microscope image of h-BN–encapsulated MoS_2/WSe_2 device (sample 1). (b) Illustration of multiple IX energy levels in moiré potential trap resulting in multiple PL peaks ($p1$-$p4$). (c) IX PL spectrum under CW excitation. The black line is the measured IX PL spectrum, and the orange line is the fitting result using four Gaussian peaks [FWHM around 30 to 60 nm (25 to 45 meV)], each shown with a different color. The intensity is in counts/s (cps). (d) Power dependence of the PL spectrum under pulse excitation.

angle compared to the case with the same chalcogen in the two layers. Because of the type II band alignment in this structure, the electrons and holes are separated into the MoS_2 and the WSe_2 layers, respectively, forming the IX with an emission wavelength of around 1200 nm [50–52].

Figure 1(b) shows a schematic of the multiple IX levels in a moiré potential trap [24]. Similar to the case of quantum dots [53], multiple bound states can exist for a deep enough potential trap. Figure 1(c) shows the IX PL spectrum obtained from the sample under 532 nm continuous wave (CW) excitation, while Fig. 1(d) shows the PL under pulse excitation (see Sec. S1 in SM [35] for discussion of the difference between the IX PL spectrum under pulse and CW excitation). The excitation beam used in this Letter has a diameter of ~1 μm with an excitation intensity of less than 2.5 kW/cm^2. All measurements were performed at 4.5 K unless noted otherwise. In both CW and pulse cases, the spectrum exhibits four peaks, indicating the multiple energy levels of IX [21–23,25,28]. We also check the CW PL spectrum under 726 nm excitation (Fig. S2 in Ref. [35]) and found that it is qualitatively similar to the one shown in Fig. 1(c). Additionally, the intralayer exciton PL spectra do not show a power-dependent energy shift (Fig. S3 in Ref. [35]), indicating that the light-induced doping is not significant in our case. As shown in Fig. 1(d), the multiple peaks appear regardless of the excitation power. The power dependence of the integrated intensity shows a sublinear behavior [see Fig. S4(b) in Ref. [35]], agreeable with previous reports [54,55]. Furthermore, at excitation power <1 μW, the energies of the exciton peaks increase with increasing power [see Fig. S4(a) in Ref. [35]]—a signature of dipolar interaction between localized IXs [55,56]. Such interaction may also explain the significant power dependence of intensity ratio between different peaks at the low power regime [see Sec. S1 and Fig. S5(a) in Ref. [35]]. We note that, based on this blueshift, the estimated maximum IX density is ~1.19×10^{12} cm^{-2}, which is below the moiré site density (1.52×10^{12} cm^{-2}) (see Sec. S2 in Ref. [35]).

The PL spectra at different excitation locations share the same qualitative characteristics [Fig. S6(a) in Ref. [35]] and we also did not use any patterned substrate [57,58] or apply external strain by other means [59], indicating that the multiple peaks feature is due to moiré superlattice instead of the disorder and externally induced strain effect [60]. Considering that the energy difference between the IX is around 30 meV, a total of four IX peaks can exist in a trap with a depth of more than 120 meV, agreeable with the theoretical upper bound of 200 meV (see Secs. S2 and S4 in Ref. [35]).

The transitions between the IX states should result in the time correlation between the emissions from different energy levels. To study this, we performed the energy- and time-resolved PL measurement by exciting the sample with a pulsed laser at 726 nm. The excited WSe_2 excitons relax in the femtosecond-to-picosecond timescale to become IX [61–63]. We then apply optical filters to study the time-resolved PL from different IX energy levels [see Fig. 2(a)]. The emissions from $p1$ and $p2$ are obtained using 1175 and 1225 nm bandpass filters in the collection arm, respectively, while the combined emission from $p3$ and $p4$ is obtained using a 1250 nm longpass filter. We also have measured emission from $p4$ using 1300 nm bandpass filter (see the filtered spectrum in Fig. S7 in Ref. [35]). However, we found that the time-resolved PL of $p3 + p4$ and $p4$ are similar (Fig. S16 in Ref. [35]). Because of this similarity, we only discuss $p3 + p4$ emission in the main text. Further discussion on $p3$ and $p4$ is presented in SM Sec. S5 [35]. Time-resolved PL measurement at another excitation location also shows a similar result [Fig. S6(b) in Ref. [35]].

We observed that: (1) all IX emissions show finite delay to reach the maximum PL count, (2) the delay time of different peaks are different, with the delay time of $p2$ ($p3 + p4$) being similar to the fast decay time of $p1$ ($p2$), (3) there are two decays components with nanosecond (ns) and microsecond (μs) timescales, respectively (the semilog plot is plotted in Figs. S8 and S13 in Ref. [35]), and (4) different peaks [$p1$, $p2$, and ($p3 + p4$)] have different fast and slow decay rates.

Here, we emphasize that the full width at half maximum (FWHM) of our excitation pulse is less than 500 picoseconds (ps) (see the impulse response function in Fig. S9 in Ref. [35]), while all the emission peaks in Fig. 2(a) are delayed more than 1.5 ns after the excitation pulse ends. Hence, these delays cannot be attributed to the finite pulse width. Similar phenomena are observed in other samples [see Ref. [35], Fig. S10 for sample 2 with an AA-stacking alignment [Fig. S1(b)] and Fig. S14(a) for sample 3]. Further discussion on the twist angle dependence is presented in Ref. [35] Sec. S6.

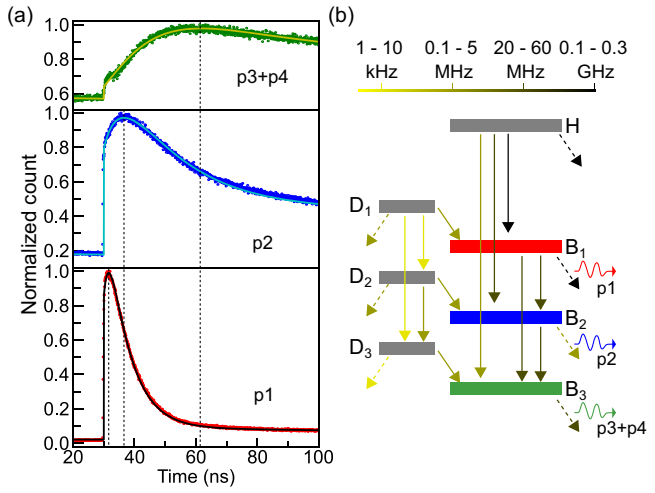

FIG. 2. (a) Energy- and time-resolved IX PL with average excitation power of 3.88 μW. The symbols are the measured data, while the lines are fitting results using the model in B. The $p1$-$p4$ is as in Fig. 1. The dashed lines indicate the peak position of each emission. The excitation pulse ends at time ∼30 ns (see Fig. S9 in Supplemental Material [35]). The normalization is done by dividing by the maximum count of each time-resolved PL data. (b) Rate equation model of IXs transitions. The solid lines indicate transitions between excited states, while the dashed lines are transitions to the ground state. Darker lines indicate faster rates following the color scale. The $D1(B1)$-$D3(B3)$ are dark (bright) IXs, while H is the high-energy state. For the power range considered in the simulation (0.46 to 17.45 μW), all transition rates are power independent.

Figure 2(b) shows the rate equation model derived from the observations above. It consists of three bright IXs ($B1$ to $B3$), three dark ones ($D1$ to $D3$), and one high energy state (H). While the exact nature of the H and dark states are not yet clear, one of the possibilities is that the H state is the hot exciton state and the dark states are either momentum- or spin-darks states (further discussion on the H and dark states is presented in Ref. [35] Sec. S6). For the power range considered in the simulation ($0.46 - 17.45$ μW), all transition rates are power independent. We note here that, since the $p3$ and $p4$ are detected together in the time-resolved experiment, the two bright states corresponding to these transitions are treated as one state ($B3$). Hence, only three bright states are considered in the model instead of four. For a similar reason, only three dark states are considered.

A delayed IX emission [point (1)] means that there are transitions from higher energy states to bright states. The transition from H to $B1$ (i.e., the highest energy bright IX) is responsible for the delay observed in $p1$ (i.e., transition from $B1$ to ground state). Similarly, the delays observed in $p2$ (i.e., $B2$-to-ground) are caused by the $B1$-to-$B2$ or H-to-$B2$ transitions. In such cascade transitions, the decrease in the higher-energy emission intensity is accompanied by the increase in the lower-energy emission intensity. This process explains why the delay in low energy emission is the same as the decay time constant of the higher one [point (2)]. The two decay components [point (3)] can be attributed to the nanosecond lifetime of the bright states decay observed and the microsecond lifetime of the dark states. More precisely, it is attributed to the dark-to-bright-to-ground decay pathway. Three dark states are needed because there are three different slow time constants [point (4)].

To verify this model, we fit the model to the experimental data with the transition rates and the initial population (right after the excitation pulse ends) of each level as the fitting parameters. The strength of the transition rate varies by several orders and is illustrated by the darkness of the lines in Fig. 2(b) (see Table S1 in Ref. [35] for the detailed transition rate values). The fitting results of the time-resolved PL are shown as lines in Fig. 2(a), which agree well with the experimental data. Fitting results at excitation powers between 0.5 to 20 μW also show a good agreement between the model and the data (see Figs. S11, S12, and S13 in Ref. [35]), supporting the existence of cascade transitions between the IX energy levels. Furthermore, the power independence of the decay rates indicates that, within this power range, the single exciton decay process dominates over the exciton-exciton annihilation (e.g., via Auger recombination [64]).

The demonstration of cascade transition here only depends on the correlation between the IX emissions and does not depend on whether the transition is radiative or not. In a way, this is a more decisive proof of cascade transition than detecting photons with energy equal to IX spacing (i.e., ∼40 μm) since that energy may correspond to other processes such as bright-dark splitting of WSe_2 intralayer exciton [65].

Another interesting phenomenon can be observed from the time-resolved PLs at high excitation power (e.g., 17.45 μW). Remarkably, instead of the count increase, we see the count rate for $(p3 + p4)$ emission drops right after the excitation laser pulse, as shown in Fig. 3(a). Similar drops are also observed for other excitation powers larger than 10 μW [see Figs. S11(e) and S11(f) and Figs. S12(e) and S12(f) in Ref. [35]]. This drop shows a possibility that the excitation pulse pumps out the residual exciton population from the previous pulse, i.e., the excited state absorption (ESA).

The nonzero residual population results in the finite count in the time-resolved PL even before the beginning of the pulse (i.e., at time <30 ns). This residual population depends on pulsed laser excitation power and repetition rate. In particular, the residual population is significant if the repetition rate is larger than the emission decay rate. Considering that the slow decay part of $(p3 + p4)$ emission is mainly determined by the $D3$-to-$B3$ transition rate of ∼0.5 MHz (see Table S1 in Ref. [35]), it is expected that the residual population is significant for a repetition rate of 2.5 MHz used in Fig. 3.

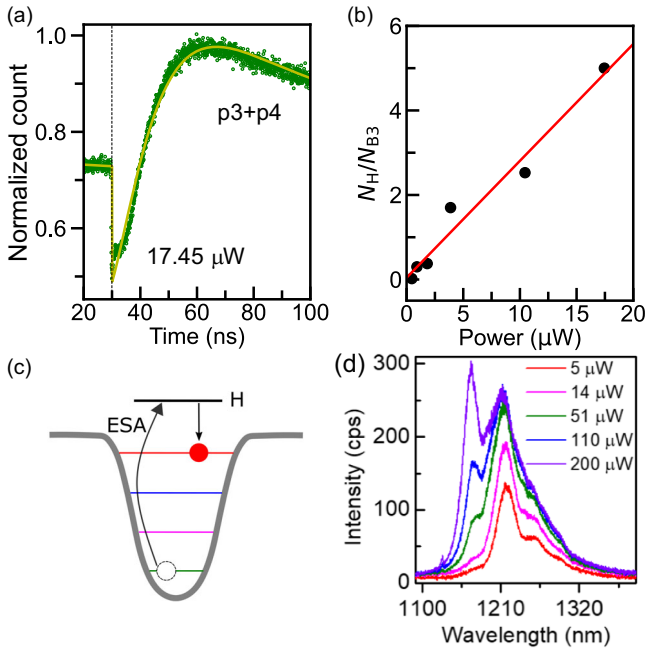

FIG. 3. (a) Time-resolved IX PL of $(p3 + p4)$ emission with average excitation power of 17.45 μW. The symbols are the measured data, while the lines are fitting results using the model in 2(b). The dotted line indicates the end of the excitation pulse. The excitation pulse decreases the emission count. (b) The ratio between $B3$ and H population at the initial time (after the end of previous excitation pulse) vs excitation power. The symbol is the result obtained from the fitting using the model in Fig. 2(b). The error bar is smaller than the symbol size. The line is linear fitting. (c) Population inversion due to ESA. (d) PL spectra under 532 nm CW excitation at various powers.

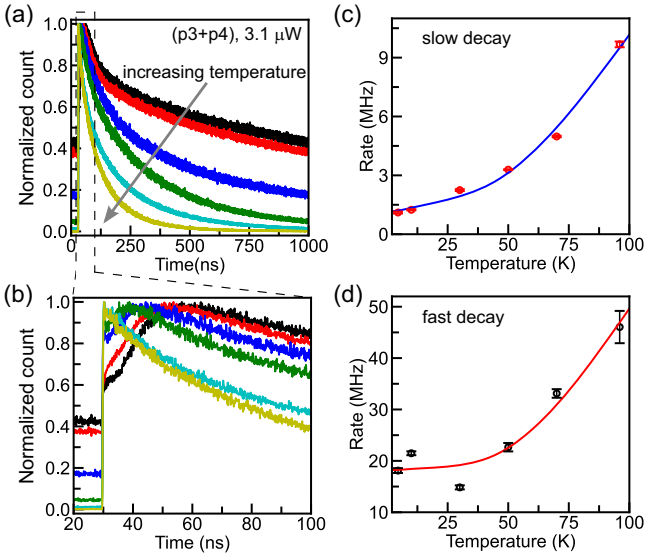

FIG. 4. (a) Time-resolved PL of $(p3 + p4)$ emission with an average excitation power of 3.1 μW at various temperatures. The temperatures are 4.5, 10, 30, 50, 70, and 96 K. (b) Close-up of (a). (c) Slow and (d) fast decay rates. The symbols are obtained from the double exponential fitting of the decaying part of (a). The error bars represent a 95% confidence interval. The solid lines are based on the theoretical model.

We next discuss possible transitions corresponding to the hypothesized ESA. Since the pulse excitation energy (~1.71 eV) is much higher than the energy difference between these IXs (~30 meV), the ESA is unlikely to happen between the IXs. Considering the energy levels in Fig. 2(b), the ESA can only be attributed to the transition to the H state. To further check this ESA process, we note that the ratio between the population of $B3$ and H state at the end of an excitation pulse (i.e., residual population) when there is ESA between $B3$ and H can be expressed as

$$N_H/N_{B3} = \alpha_{BH}P + \alpha_{0H}, \tag{1}$$

where $N_{H(B3)}$ is the population of H ($B3$) state at the end of the excitation pulse, P is the average excitation power, and $\alpha_{BH(0H)}$ is proportional to the $B3$ (ground)-to-H absorption rate (see more details in Ref. [35] Sec. S8). This ratio is plotted in Fig. 3(b). The ratio shows a linear dependence on excitation power, which is agreeable with Eq. (1) and the hypothesized optically excited $B3$-to-H transition.

The ESA can lead to the population inversion of IX under high enough excitation power, as illustrated in Fig. 3(c). Based on the fitting results [Fig. 2(b) and Table S1 in Ref. [35]], we note that the H-to-$B1$ transition is at least 3 orders faster than the H-to-$B3$ transition. Considering that the $B3$ can be pumped to H, this significant difference in the decay rates means that the exciton pumped from $B3$ to H will quickly decay to $B1$. Such a mechanism provides an efficient population transfer from the lower energy IX to the higher one, enabling IX population inversion. To test this, we excite the sample with 532 nm CW laser at various powers. The power-dependent PL spectra are shown in Fig. 3(d). At sufficiently high excitation power, the population of the high energy peak ($p1$, wavelength ~1170 nm) grows faster than the low energy peaks, leading toward population inversion. Indeed, CW PL spectra obtained from another sample (sample 3) conclusively show population inversion at a high excitation power [Fig. S14(c) in Ref. [35]].

Finally, we discuss the effect of temperature on the cascade transition's optical signature (i.e., the delayed emission of IX). The time-resolved PL of $(p3 + p4)$ emission with an excitation power of 3.1 μW at temperatures ranging from 4.5 to 96 K are shown in Figs. 4(a) and 4(b). Similar plots for other peaks are shown in Fig. S15 in Ref. [35]. Figure 4(b) shows that the τ_{delay} (i.e., the delay between the PL peak and the pulse stop) decreases with increasing temperature. Eventually, the rising time vanishes at temperatures above 70 K.

The temperature dependence can be explained by considering that fast and slow decay rates increase with

increasing temperature [Figs. 4(c) and 4(d)]. The emitting state's outgoing population rate increases as these rates increase, reducing its population growth. As a result, the maximum count is reached at an earlier time. The temperature dependence of the decay rates can be understood as the result of the increase in phonon-assisted exciton decay rate with increasing temperature. As shown in Figs. 4(c) and 4(d), the data agree well with the theoretical model taking into account this phonon-assisted exciton decay mechanism (see Ref. [35] Sec. S9 for more details on this model).

In summary, by performing energy- and time-resolved PL measurements, we observe the cascade transition between IXs in MoS_2/WSe_2 moiré superlattices, as indicated by the correlation between different IX emissions. Furthermore, we demonstrate an efficient population transfer from the lower-energy IX to the higher one, possibly through ESA, leading to the IX population inversion. Future studies could be done on studying the radiative nature of the reported cascade transitions. Considering that the cascade transition energy is ~10 THz, such a study could result in a moiré-based terahertz QCL. The in-plane periodic quantum confinement in such moiré-based QCL supports in-plane polarized emission, compatible with vertical-cavity surface-emitting laser architecture [66]. Additionally, when the IX emission can be driven into the single-photon regime, the radiative IX cascade transition can be used to generate entangled photon pairs [31]. On the other hand, the hypothesized ESA shows that the bright IX population can be driven to one quantum state. Such capability could be exploited for realizing high-temperature exciton condensate [29] or bosonic Mott insulator [67]. Our findings thus open up new possibilities to realize novel light sources and many-body quantum states based on moiré superlattices.

This work is supported by the Singapore National Research Foundation through its Competitive Research Program (CRP Awards No. NRF-CRP22-2019-0004, No. NRF-CRP23-2019-0002, and Quantum engineering programme) and Singapore Ministry of Education [MOE2016-T3-1-006 (S)].

*Q. T. and A. R. contributed equally to this work.
†Corresponding author.
kostya@nus.edu.sg
‡Corresponding author.
wbgao@ntu.edu.sg

[1] K. Kim *et al.*, Nano Lett. **16**, 1989 (2016).
[2] G. Li, A. Luican, J. M. B. Lopes dos Santos, A. H. Castro Neto, A. Reina, J. Kong, and E. Y. Andrei, Nat. Phys. **6**, 109 (2010).
[3] A. M. van der Zande *et al.*, Nano Lett. **14**, 3869 (2014).
[4] J. Xue, J. Sanchez-Yamagishi, D. Bulmash, P. Jacquod, A. Deshpande, K. Watanabe, T. Taniguchi, P. Jarillo-Herrero, and B. J. LeRoy, Nat. Mater. **10**, 282 (2011).
[5] C. Zhang, C.-P. Chuu, X. Ren, M.-Y. Li, L.-J. Li, C. Jin, M.-Y. Chou, and C.-K. Shih, Sci. Adv. **3**, e1601459 (2017).
[6] L. Esaki and R. Tsu, IBM J. Res. Dev. **14**, 61 (1970).
[7] R. Bistritzer and A. H. MacDonald, Proc. Natl. Acad. Sci. U.S.A. **108**, 12233 (2011).
[8] E. Suárez Morell, J. D. Correa, P. Vargas, M. Pacheco, and Z. Barticevic, Phys. Rev. B **82**, 121407(R) (2010).
[9] F. Wu, T. Lovorn, E. Tutuc, and A. H. MacDonald, Phys. Rev. Lett. **121**, 026402 (2018).
[10] Z. Zhang, Y. Wang, K. Watanabe, T. Taniguchi, K. Ueno, E. Tutuc, and B. J. LeRoy, Nat. Phys. **16**, 1093 (2020).
[11] Y. Pan, S. Fölsch, Y. Nie, D. Waters, Y.-C. Lin, B. Jariwala, K. Zhang, K. Cho, J. A. Robinson, and R. M. Feenstra, Nano Lett. **18**, 1849 (2018).
[12] L. A. Ponomarenko *et al.*, Nature (London) **497**, 594 (2013).
[13] C. R. Dean *et al.*, Nature (London) **497**, 598 (2013).
[14] Q. Tong, H. Yu, Q. Zhu, Y. Wang, X. Xu, and W. Yao, Nat. Phys. **13**, 356 (2017).
[15] M. Fox and R. Ispasoiu, in *Springer Handbook of Electronic and Photonic Materials*, edited by S. Kasap and P. Capper (Springer US, Boston, MA, 2017), pp. 1021, 10.1007/978-3-319-48933-9_55.
[16] A. Splendiani, L. Sun, Y. Zhang, T. Li, J. Kim, C.-Y. Chim, G. Galli, and F. Wang, Nano Lett. **10**, 1271 (2010).
[17] K. F. Mak, C. Lee, J. Hone, J. Shan, and T. F. Heinz, Phys. Rev. Lett. **105**, 136805 (2010).
[18] G. Wang, A. Chernikov, M. M. Glazov, T. F. Heinz, X. Marie, T. Amand, and B. Urbaszek, Rev. Mod. Phys. **90**, 021001 (2018).
[19] F. Wu, T. Lovorn, and A. H. MacDonald, Phys. Rev. Lett. **118**, 147401 (2017).
[20] S. Brem, C. Linderälv, P. Erhart, and E. Malic, Nano Lett. **20**, 8534 (2020).
[21] C. Jin *et al.*, Nature (London) **567**, 76 (2019).
[22] E. M. Alexeev *et al.*, Nature (London) **567**, 81 (2019).
[23] K. Tran *et al.*, Nature (London) **567**, 71 (2019).
[24] F. Wu, T. Lovorn, and A. H. MacDonald, Phys. Rev. B **97**, 035306 (2018).
[25] J. Choi, M. Florian, A. Steinhoff, D. Erben, K. Tran *et al.*, Phys. Rev. Lett. **126**, 047401 (2021).
[26] H. Yu, G.-B. Liu, J. Tang, X. Xu, and W. Yao, Sci. Adv. **3**, e1701696 (2017).
[27] X. Lu, X. Li, and L. Yang, Phys. Rev. B **100**, 155416 (2019).
[28] K. L. Seyler, P. Rivera, H. Yu, N. P. Wilson, E. L. Ray, D. G. Mandrus, J. Yan, W. Yao, and X. Xu, Nature (London) **567**, 66 (2019).
[29] Z. Wang, D. A. Rhodes, K. Watanabe, T. Taniguchi, J. C. Hone, J. Shan, and K. F. Mak, Nature (London) **574**, 76 (2019).
[30] H. Baek, M. Brotons-Gisbert, Z. X. Koong, A. Campbell, M. Rambach, K. Watanabe, T. Taniguchi, and B. D. Gerardot, Sci. Adv. **6**, eaba8526 (2020).
[31] N. Akopian, N. H. Lindner, E. Poem, Y. Berlatzky, J. Avron, D. Gershoni, B. D. Gerardot, and P. M. Petroff, Phys. Rev. Lett. **96**, 130501 (2006).
[32] A. Kiraz, S. Fälth, C. Becher, B. Gayral, W. V. Schoenfeld, P. M. Petroff, L. Zhang, E. Hu, and A. Imamoğlu, Phys. Rev. B **65**, 161303(R) (2002).
[33] J. Faist, F. Capasso, D. L. Sivco, C. Sirtori, A. L. Hutchinson, and A. Y. Cho, Science **264**, 553 (1994).

[34] P. Schmidt *et al.*, Nat. Nanotechnol. **13**, 1035 (2018).
[35] See Supplemental Material at http://link.aps.org/supplemental/10.1103/PhysRevLett.129.247401 for more data and analysis of data, which includes Refs. [36–49].
[36] J. Kang, S. Tongay, J. Zhou, J. Li, and J. Wu, Appl. Phys. Lett. **102**, 012111 (2013).
[37] Y. Ding, Y. Wang, J. Ni, L. Shi, S. Shi, and W. Tang, Physica B (Amsterdam) **406**, 2254 (2011).
[38] F. A. Rasmussen and K. S. Thygesen, J. Phys. Chem. C **119**, 13169 (2015).
[39] C. Gong, H. Zhang, W. Wang, L. Colombo, R. M. Wallace, and K. Cho, Appl. Phys. Lett. **103**, 053513 (2013).
[40] H. Li *et al.*, Nat. Mater. **20**, 945 (2021).
[41] M. H. Naik *et al.*, Nature (London) **609**, 52 (2022).
[42] S. Shabani, D. Halbertal, W. Wu, M. Chen, S. Liu, J. Hone, W. Yao, D. N. Basov, X. Zhu, and A. N. Pasupathy, Nat. Phys. **17**, 720 (2021).
[43] C. N. Lau, M. W. Bockrath, K. F. Mak, and F. Zhang, Nature (London) **602**, 41 (2022).
[44] J. Binder *et al.*, Nat. Commun. **10**, 2335 (2019).
[45] K.-Q. Lin *et al.*, Nat. Commun. **12**, 5500 (2021).
[46] A. Kormányos, V. Zólyomi, N. D. Drummond, P. Rakyta, G. Burkard, and V. I. Fal'ko, Phys. Rev. B **88**, 045416 (2013).
[47] T. Cheiwchanchamnangij and W. R. L. Lambrecht, Phys. Rev. B **85**, 205302 (2012).
[48] E. S. Kadantsev and P. Hawrylak, Solid State Commun. **152**, 909 (2012).
[49] S. Fiore and M. Luisier, Phys. Rev. Mater. **4**, 094005 (2020).
[50] O. Karni *et al.*, Phys. Rev. Lett. **123**, 247402 (2019).
[51] Q. Tan, A. Rasmita, S. Li, S. Liu, Z. Huang, Q. Xiong, S. A. Yang, K. S. Novoselov, and W.-b. Gao, Sci. Adv. **7**, eabh0863 (2021).
[52] Y. Liu, H. Fang, A. Rasmita, Y. Zhou, J. Li, T. Yu, Q. Xiong, N. Zheludev, J. Liu, and W. Gao, Sci. Adv. **5**, eaav4506 (2019).
[53] T. V. Torchynska, M. Dybiec, and S. Ostapenko, Phys. Rev. B **72**, 195341 (2005).
[54] W. Li, X. Lu, J. Wu, and A. Srivastava, Nat. Nanotechnol. **16**, 148 (2021).
[55] M. Brotons-Gisbert, H. Baek, A. Campbell, K. Watanabe, T. Taniguchi, and B. D. Gerardot, Phys. Rev. X **11**, 031033 (2021).
[56] W. Li, X. Lu, S. Dubey, L. Devenica, and A. Srivastava, Nat. Mater. **19**, 624 (2020).
[57] M. Kremser *et al.*, npj 2D Mater. Appl. **4**, 8 (2020).
[58] A. R. P. Montblanch *et al.*, Commun. Phys. **4**, 119 (2021).
[59] Y. Bai *et al.*, Nat. Mater. **19**, 1068 (2020).
[60] F. Mahdikhanysarvejahany *et al.*, Nat. Commun. **13**, 5354 (2022).
[61] H. Zhu, J. Wang, Z. Gong, Y. D. Kim, J. Hone, and X. Y. Zhu, Nano Lett. **17**, 3591 (2017).
[62] J. E. Zimmermann, M. Axt, F. Mooshammer, P. Nagler, C. Schüller, T. Korn, U. Höfer, and G. Mette, ACS Nano **15**, 14725 (2021).
[63] X. Hong, J. Kim, S.-F. Shi, Y. Zhang, C. Jin, Y. Sun, S. Tongay, J. Wu, Y. Zhang, and F. Wang, Nat. Nanotechnol. **9**, 682 (2014).
[64] J. Wang, J. Ardelean, Y. Bai, A. Steinhoff, M. Florian, F. Jahnke, X. Xu, M. Kira, J. Hone, and X.-Y. Zhu, Sci. Adv. **5**, eaax0145 (2019).
[65] X.-X. Zhang *et al.*, Nat. Nanotechnol. **12**, 883 (2017).
[66] W. Nakwaski, M. Dems, R. P. Sarzała, S. Grzempa, and T. Czyszanowski, in *2018 20th International Conference on Transparent Optical Networks (ICTON)* (2018), p. 1, 10.1109/ICTON.2018.8473721.
[67] C. Lagoin, S. Suffit, K. Baldwin, L. Pfeiffer, and F. Dubin, Nat. Phys. **18**, 149 (2022).